Improved carrier concentration control in Zn-doped $Ca_5Al_2Sb_6$

Alex Zevalkink,[1] Eric S. Toberer,[1] Tim Bleith,[1] Espen Flage-Larsen,[2] and G. Jeffrey Snyder[1,a)]
[1]*Materials Science, California Institute of Technology, 1200 E. California Blvd., Pasadena, California 91125, USA*
[2]*Physics Department, Colorado School of Mines, 1500 Illinois St., Golden, Colorado 80401, USA*

(Received 1 April 2011; accepted 1 June 2011; published online 14 July 2011)

$Ca_5Al_2Sb_6$ is an inexpensive, Earth-abundant compound that exhibits promising thermoelectric efficiency at temperatures suitable for waste heat recovery. Inspired by our previous study of *p*-type $Ca_{5-x}Na_xAl_2Sb_6$, this work investigates doping with Zn^{2+} on the Al^{3+} site ($Ca_5Al_{2-x}Zn_xSb_6$). We find Zn to be an effective *p*-type dopant, in contrast to the low solubility limit and poor doping efficiency of Na. Seebeck coefficient measurements indicate that the hole band mass is unaffected by the dopant type in the high-zT temperature range. Band structure and density of states calculations are employed in order to understand the carrier concentration-dependent effective mass. $Ca_5Al_{2-x}Zn_xSb_6$ has a low lattice thermal conductivity that approaches the predicted minimum value at high temperature (1000 K) due to the complex crystal structure and high mass contrast. © *2011 American Institute of Physics*. [doi:10.1063/1.3607976]

INTRODUCTION

Thermoelectric materials, used to convert heat to electricity, have the potential to reduce the huge quantity of energy that is currently lost in the form of high quality waste heat.[1] Today, the widespread implementation of thermoelectric devices to capture some of this lost energy is limited largely by the toxicity and expense of the most efficient thermoelectric materials. Efficiency in thermoelectric generators is limited by the figure of merit ($zT = \alpha^2 T/\rho\kappa$), which depends on the Seebeck coefficient (α), the electrical resistivity (ρ), and the thermal conductivity (κ).[2]

Zintl compounds are a promising class of compounds for inexpensive and non-toxic thermoelectric materials.[3] These compounds contain both covalent and ionic bonding, resulting in an extensive variety of structures and options for chemical substitution. High thermoelectric efficiency has been demonstrated in a number of Zintl compounds ($CsBi_4Te_6$, $Yb_{14}MnSb_{11}$, Ca_3AlSb_3, AZn_2Sb_2).[4–11]

One promising new Zintl compound is $Ca_5Al_2Sb_6$, which shows a peak zT of 0.6 at 1000 K with Na^{1+} doping on the Ca^{2+} site.[13] A prior investigation revealed $Ca_5Al_2Sb_6$ to be a narrow band-gap semiconductor (0.5 eV) with exceptionally low lattice thermal conductivity (0.6 W m^{-1} K^{-1} at 800 K). The semiconducting character of $Ca_5Al_2Sb_6$ arises from the valence-precise nature of the chemical bonding. The crystal structure of $Ca_5Al_2Sb_6$ is shown in Fig. 1. $Ca_5Al_2Sb_6$ (*Pbam*) is composed of infinite parallel chains of $AlSb_4$ tetrahedra with Sb–Sb bonds linking the chain moieties together, resulting in ladder-like structures.[12] Many isostructural analogs of $Ca_5Al_2Sb_6$ exist, and a few have been studied for their electronic properties.[14–16] The complex structure (26 atoms in the primitive cell) and high mass contrast lead to low velocity phonon modes and the associated low lattice thermal conductivity.

Although Na-doping in $Ca_5Al_2Sb_6$ successfully yielded degenerate behavior, a solubility limit was reached at a doping level of 2×10^{20} h^+ cm^{-3}, and the dopant effectiveness was low.[13] Inspired by our previous investigation of the thermoelectric properties of Zn-doped $Yb_{14}MnSb_{11}$, here we consider $Ca_5Al_{2-x}Zn_xSb_6$ ($x = 0$, 0.02, 0.05, 0.10, and 0.20).[17] Zn is an attractive dopant due to its low cost and ease of handling. A combination of high temperature transport measurements and classic transport theory is used to compare the effects of Na- and Zn-doping in $Ca_5Al_2Sb_6$. This work is complemented by electronic structure calculations of the $Ca_5Al_2Sb_6$ parent phase.

EXPERIMENTAL DETAILS

Bulk polycrystalline $Ca_5Al_{2-x}Zn_xSb_6$ ($x = 0$, 0.02, 0.05, 0.10, 0.20) samples were prepared by ball milling followed by hot pressing. Starting with 99.99% pure Ca dendrites from Sigma-Aldrich and 99.99% Zn shot, 99% Al shot, and 99.5%

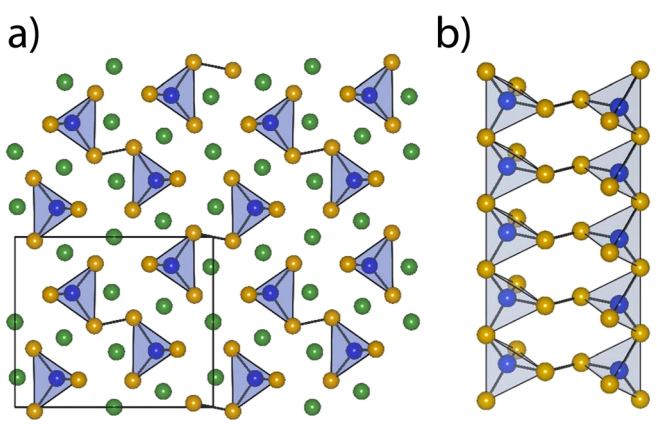

FIG. 1. (Color online) (a) $Ca_5Al_2Sb_6$ orthorhombic unit cell (*Pbam*) viewed along the [001] direction. (b) Covalent substructure formed from infinite chains of corner sharing $AlSb_4$ tetrahedra connected via Sb–Sb bonds. Sb atoms are orange, Ca are green, and Al are blue (Ref. 12).

a)Author to whom correspondence should be addressed. Electronic mail: jsnyder@caltech.edu.

Sb lumps from Alpha Aesar, the elements were loaded into stainless-steel vials with stainless-steel balls in an argon-filled glovebox. The reagents were milled for 60 min using a SPEX Sample Prep 8000 Series Mixer/Mill. The resulting powder was consolidated in an inductive hot press[18] in high density graphite dies (POCO) using 40 MPa of pressure. A maximum temperature of 873 K was used during hot pressing for 5 h in argon, followed by a 3 h cooldown. Descriptions of the chemical, thermal, and electronic characterization techniques used in this study can be found in Ref. 6.

Electronic transport measurements were analyzed using solutions to the Boltzmann transport equation within the relaxation time approximation, and assuming a single, parabolic band, as described in Ref. 13. Electronic structure calculations were performed in the Vienna Ab-initio Simulation Package (VASP).[19,20] For the exchange and correlation, the Perdew-Burke-Enzerhof generalized gradient approximation[21] functional was used in the projector augmented-wave formalism.[22] The experimental lattice constants and atom positions reported by Cordier *et al.* were used as input.[12] A *k*-point grid of $4 \times 4 \times 12$ and an energy cutoff of 400 eV were necessary in order to converge the total energy to within a few meV.

RESULTS AND DISCUSSION

Following ball milling and hot pressing, $Ca_5Al_{2-x}Zn_xSb_6$ samples ($x = 0, 0.02, 0.05, 0.10, 0.20$) have geometric densities ranging from 91% to 97% and are found to be phase pure by x-ray diffraction (Fig. 2) and scanning electron microscopy (SEM). SEM analysis of fracture surfaces reveals small grains (1 μm in diameter) and porosity (0.1 μm in diameter) at grain boundaries. The larger grain size (50 μm) and slightly higher density ($\geq$98%) found in the Na-doped samples are due to the use of a higher hot-pressing temperature (973 K) and pressure (100 MPa) as compared with the current study.

Electronic transport properties

Undoped $Ca_5Al_2Sb_6$ is expected to be an intrinsic semiconductor from Zintl valence-counting rules. Upon doping, each Zn^{2+} atom on an Al^{3+} site is expected to contribute one free hole. As shown in Fig. 3, the measured room temperature

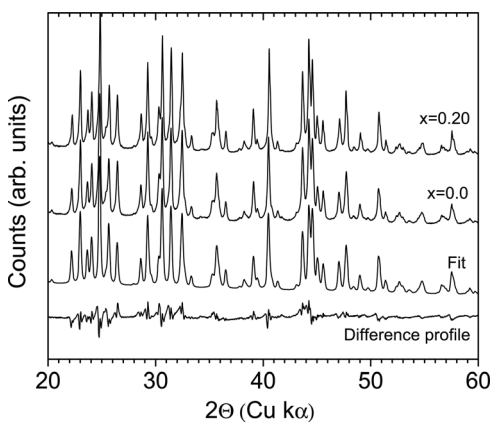

FIG. 2. $Ca_5Al_{2-x}Zn_xSb_6$ x-ray diffraction patterns ($x = 0, 0.20$), Reitveld fit to the $x = 0$ sample, and associated difference profile. No secondary phases are observed for the x range investigated ($0 < x < 0.20$).

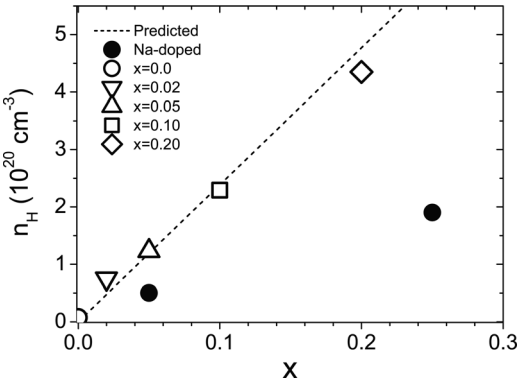

FIG. 3. With zinc doping, the carrier concentration at 300 K is directly proportional to the level predicted using simple electron counting (dashed line). This is in contrast to the lower doping efficiency with sodium (Ref. 13).

Hall carrier concentration (n_H) in $Ca_5Al_{2-x}Zn_xSb_6$ is very close to that predicted (dashed line) as a function of the Zn content (x). This is in sharp contrast to the measured hole concentrations in $Ca_{5-x}Na_xAl_2Sb_6$, which are significantly lower than predicted. The maximum hole concentration obtained in Zn-doped $Ca_5Al_2Sb_6$ is twice that obtained by doping with Na.

Figure 4 shows high temperature Hall measurements for $Ca_5Al_{2-x}Zn_xSb_6$ samples, as well as those for $Ca_{4.75}Na_{0.25}Al_2Sb_6$ from our previous work. The Hall carrier concentration (Fig. 4(a)) of the un-doped sample increases with increasing temperature, likely due to minority carrier activation beginning at 400 K. The anomaly in the resistivity at 850 K requires further investigation, but it might be due to a phase change. In the doped samples, the carrier concentration remains nearly constant with increasing temperature, indicative of degenerate carrier behavior.

The Hall mobility (Fig. 4(b)) as a function of temperature is calculated from the measured Hall coefficient and the resistivity (ρ). When scattering by acoustic phonons dominates, the temperature dependence of μ is described by $\mu_a \propto T^{-\nu_a}$, where ν_a is predicted to be 1 to 1.5 for degenerate and non-degenerate semiconductors, respectively.[23] In the case of undoped $Ca_5Al_2Sb_6$, the mobility can be fit using $\nu_a = 1.5$, as shown in Fig. 4(b). Compared with the undoped and Na-doped $Ca_5Al_2Sb_6$, the mobility in the Zn-doped samples is suppressed at low temperatures (300-600 K) and rises slightly with increasing temperature. Increasing mobility with increasing temperature was also observed in the related Ca_3AlSb_3 compound.[6] This behavior was found in both undoped and doped Ca_3AlSb_3 samples and fit well to an activated process, suggesting a barrier at the grain boundaries.

Dramatic changes to either the carrier scattering or the band mass could lead to decreased mobility in the Zn-doped $Ca_5Al_2Sb_6$ samples. Sources of scattering could include (a) boundary scattering from pores or grain boundaries, (b) activation barriers at grain boundaries ($\mu_{act} \propto e^{E_A/\kappa T}$), (c) local strain fields,[24] or (d) ionized impurity scattering ($\mu_i \propto T^{\nu_i}$). The temperature dependence of the mobility can be fit with a combination of acoustic phonon scattering and an activation barrier, which is consistent with the small grain size observed in the Zn-doped samples. However, further study of the microstructure and transport properties is needed in

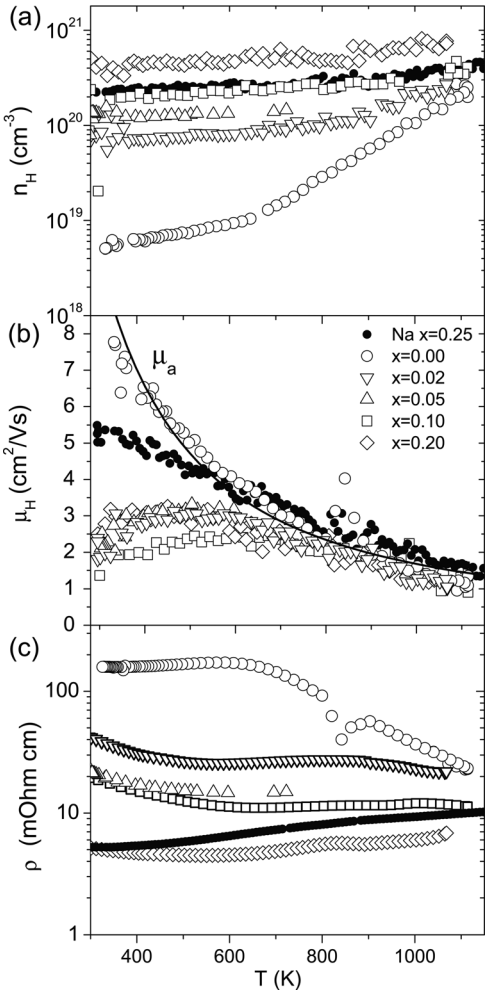

FIG. 4. (a) High temperature Hall coefficient measurements of $Ca_5Al_{2-x}Zn_xSb_6$ yield the carrier concentration. Doped samples exhibit extrinsic behavior to 800 K. (b) Undoped $Ca_5Al_2Sb_6$ exhibits a mobility dominated by phonon scattering ($\mu_a \propto T^{-1.5}$) across the entire temperature range investigated, whereas Zn-doped samples show evidence of additional scattering mechanisms at low temperature. (c) The high temperature resistivity decreases with increasing Zn doping level.

order to understand the exact role of scattering in the decreased mobility.

In order to consider the effect of Zn on the band structure, the Seebeck coefficients of Zn- and Na-doped $Ca_5Al_2Sb_6$ are considered at 700 K (Fig. 5). At this temperature, Zn- and Na-doped samples with equivalent carrier concentrations and scattering mechanisms (acoustic phonon scattering) exhibit nearly identical Seebeck coefficients. This suggests that the effective mass is unaffected by Zn doping at high temperature. The pisarenko curve in Fig. 5 was generated using a single parabolic band (SPB) model with an effective mass of 1.8 m_e, and assuming acoustic phonon scattering. It appears that for high carrier concentrations ($x = 0.2$ sample with $n_H = 4.7 \times 10^{20}$), $Ca_5Al_2Sb_6$ can no longer be described by a single parabolic band model. We do not employ this model at low temperatures, as it is difficult to unravel potential changes in the effective mass from the multiple scattering mechanisms.

The Seebeck coefficients are shown in Fig. 6 as a function of temperature. Doped samples exhibit increasing Seebeck coefficients with rising temperature, as expected for extrinsically doped semiconductors. The Seebeck coefficients of the Na-doped ($x = 0.25$) and Zn-doped ($x = 0.10$) samples are nearly identical across the entire temperature range, consistent with their similar carrier concentrations.

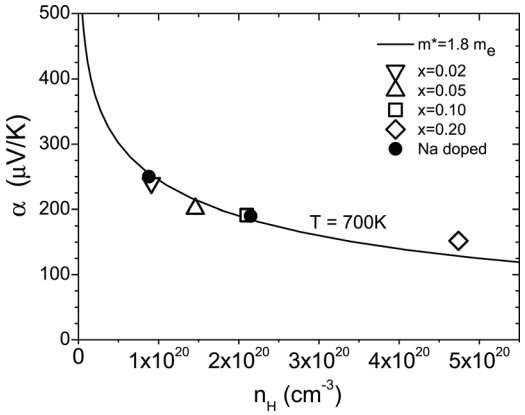

FIG. 5. Similar Seebeck coefficient values for Na- and Zn-doped $Ca_5Al_2Sb_6$ at equivalent carrier concentrations suggest similar band mass. The curve was generated using a single parabolic band approximation and an effective mass of 1.8 m_e (Ref. 13).

Electronic structure calculations

Further insight into the intrinsic electronic transport behavior is obtained from the electronic structure calculations. For thermoelectric materials, such calculations reveal the band mass, m^*_{band}, and the degeneracy, N_v, near the band edge. Here, m^*_{band} is determined by parabolic parameterization. The SPB effective masses m^* and m^*_{band} are related via the band degeneracy according to $(m^*)^{3/2} = N_v(m^*_{band})^{3/2}$. As the mobility is determined by m^*_{band}, a high band degeneracy is desirable in thermoelectric materials.[25,26]

Consistent with the experimental results above, simple electron counting suggests that $Ca_5Al_2Sb_6$ should be a semiconductor. The calculated band structure and density of states of $Ca_5Al_2Sb_6$ are shown in Fig. 7 and reveal a direct bandgap of 0.15 eV at the X point. In the upper valence and lower conduction band, the main contributions to the density of states are the Sb p- and Ca d-states. As there is a negligible

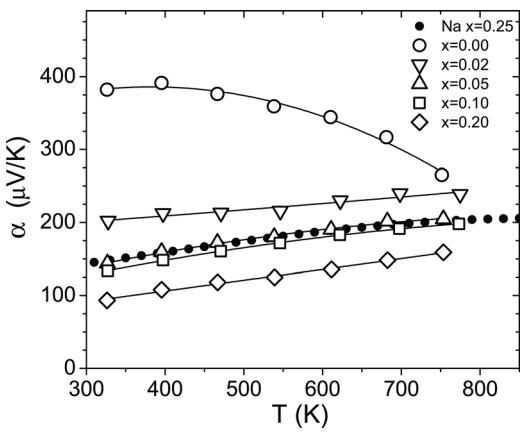

FIG. 6. High temperature Seebeck coefficients of $Ca_5Al_{2-x}Zn_xSb_6$ show degenerate behavior for the extrinsically doped, p-type compositions. Similar behavior is seen in the Na-doped analog (Ref. 13).

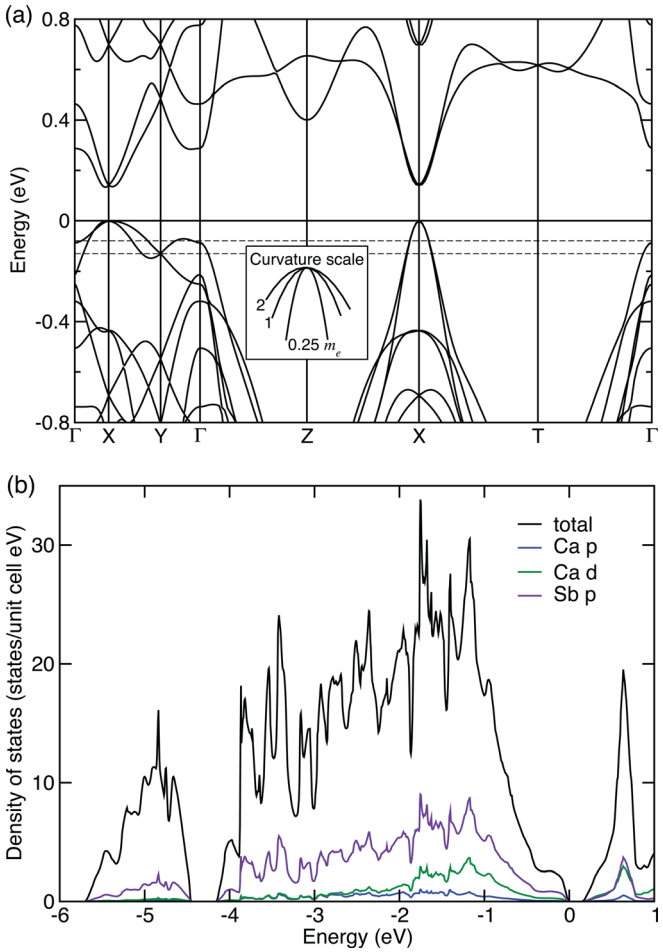

FIG. 7. (Color online) (a) The calculated $Ca_5Al_2Sb_6$ band structure shows a direct gap at *X*. The valence bandedge consists of two nested hole pockets with band masses between 0.25 and 2 m_e, depending on the direction. The dashed lines at −0.08 and −0.13 eV correspond to 1 and 5×10^{20} h^+ cm^{-3}, respectively. (b) The density of states of $Ca_5Al_2Sb_6$ shows that the material is a semiconductor with Sb *p* states as the dominant influence near the valence bandedge.

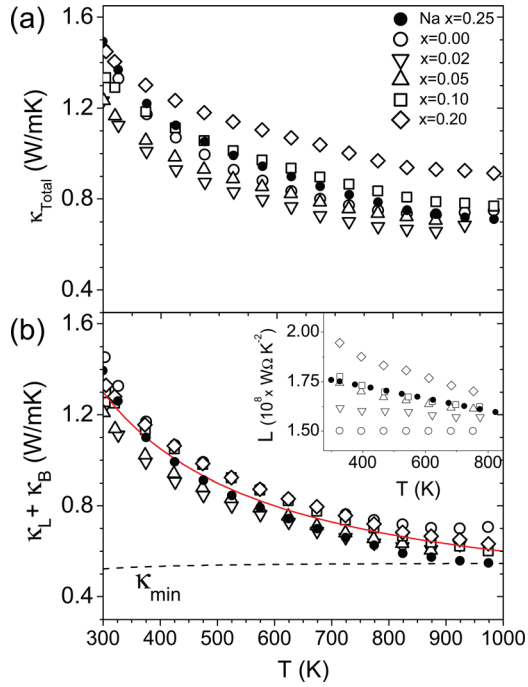

FIG. 8. (Color online) (a) The total thermal conductivity of $Ca_5Al_{2-x}Zn_xSb_6$ increases with increasing doping level and thus electronic conductivity. (b) The lattice contribution (κ_L) decays with T^{-1} and approaches a minimum value at high temperature, consistent with prior Na-doped compositions (Ref. 13). To calculate κ_L, the Lorenz coefficients (inset) were calculated using the single parabolic band approximation.

Al contribution to the band edges, rigid band behavior can be expected when Zn is substituted for Al. This is consistent with our experimental observation that Zn has a minimal effect on m^*.

The calculated band structure reveals nested bands at the *X* point, leading to a doubly degenerate band edge. An additional doubly degenerate band is found ~0.1 eV into the band, between Γ and *Y*. The energies corresponding to carrier concentrations of 1 and 5×10^{20} cm^{-3} are shown in Fig. 7. The pocket of bands at ~ −0.1 eV and the anharmonicity away from the intrinsic band edge will lead to a breakdown of the SPB model at high carrier concentrations (Fig. 5).

Thermal transport properties

The thermal conductivity, shown in Fig. 8, was calculated using $\kappa = D\delta C_p$ where the thermal diffusivity (D) is measured using the laser flash method, δ is the geometric density, and the heat capacity (C_p) is given by the Dulong-Petit value. The total thermal conductivity is a combination of electronic (κ_e), lattice (κ_L), and bipolar (κ_B) contributions. As an increasing carrier concentration leads to increased κ_e, the largest values of κ are found in the most heavily doped samples. The Wiedemann-Franz relation can be used to estimate $\kappa_e = LT/\rho$. Here, the Lorenz numbers (L) are calculated from the experimental Seebeck coefficients, using the single parabolic band approximation described in Refs. 6 and 27 and assuming a mobility limited by acoustic phonon scattering. Near room temperature, the presence of other scattering sources might alter L, but they are not accounted for in this model. As the Seebeck coefficient was measured only to 773 K, the value of L at 773 K is used to calculate κ_e at higher temperatures.

Subtracting κ_e from the total thermal conductivity yields $\kappa_L + \kappa_B$ (Fig. 8(b)). Whereas undoped $Ca_5Al_2Sb_6$ shows a slight bipolar contribution at high temperature, no such effect is seen in the the heavily doped samples.[28] These are well described by the T^{-1} relationship expected for Umklapp scattering dominated transport, as shown by the red curve in Fig. 8(b). As in Na-doped $Ca_5Al_2Sb_6$, the effect of Zn doping on the lattice thermal conductivity is negligible.

An estimated minimum thermal conductivity κ_{min} (dashed line) was calculated using Cahill's formulation for the thermal conductivity of glasses, and we used the previously reported longitudinal and transverse speeds of sound of $Ca_5Al_2Sb_6$ (4170 m/s and 2440 m/s, respectively).[13,29] For doped samples, the approach of κ_L toward the predicted glassy minimum κ_L is largely due to the structural complexity of $Ca_5Al_2Sb_6$ (26 atoms per primitive cell), which traps heat in low velocity optical phonon modes and creates additional scattering channels for Umklapp processes.[30–32]

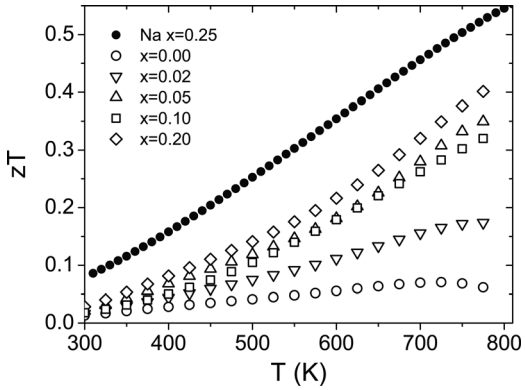

FIG. 9. As compared to sodium doped $Ca_5Al_2Sb_6$, the reduced mobility of the samples in this study lead to a lower zT. Within the Zn series, the highest doped composition exhibits the largest zT.

Figure of merit

The figure of merit for the $x = 0$-0.2 compositions, calculated from the high temperature results presented above, is shown in Fig. 9. Zn doping results in zT values that are lower than those of the sodium doped sample ($x = 0.25$). As the Zn $x = 0.1$ and Na $x = 0.25$ samples have nearly identical n_H, α, and κ_L, the overall decrease in the figure of merit is attributed solely to the reduced mobility in these Zn-doped samples. The $x = 0.2$ sample exhibits the highest zT values within the $Ca_5Al_{2-x}Zn_xSb_6$ series, suggesting that the limited doping levels available with Na-doping are insufficient to maximize performance.

CONCLUSION

Our investigation of Zn-doped $Ca_5Al_2Sb_6$ shows that this dopant provides excellent dopant effectiveness and yields higher hole carrier concentrations than were previously obtainable with Na. A similar band mass and lattice thermal conductivity is observed for both Na and Zn dopants. However, the Zn-doped samples in this study exhibit reduced carrier mobility near room temperature as compared to those subjected to Na doping, possibly due to the relative decrease in grain size. Electronic structure calculations suggest that the observed enhancement of the Seebeck coefficient at high carrier concentrations arises from a complex band structure.

ACKNOWLEDGMENTS

We gratefully acknowledge the support of the Jet Propulsion Laboratory and the National Science Foundation. Espen Flage-Larsen would also like to thank the Norwegian Research Council for financial support and the Norwegian Metacenter for Computational Science for computational resources.

[1]L. Bell, Science **321**, 1457 (2008).
[2]G. J. Snyder and E. S. Toberer, Nature Mater. **7**, 105 (2008).
[3]E. S. Toberer, A. F. May, and G. J. Snyder, Chem. Mater. **22**, 624 (2010).
[4]D.-Y. Chung, T. P. Hogan, M. Rocci-Lane, P. Brazis, J. R. Ireland, C. R. Kannewurf, M. Bastea, C. Uher, and M. G. Kanatzidis, J. Am. Chem. Soc. **126**, 6414 (2004).
[5]E. S. Toberer, C. A. Cox, S. R. Brown, T. Ikeda, A. F. May, S. M. Kauzlarich, and G. J. Snyder, Adv. Funct. Mater. **18**, 2795 (2008).
[6]A. Zevalkink, E. S. Toberer, W. Zeier, E. Flage-Larsen, and G. J. Snyder, Energy Environ. Sci. **4**, 510 (2011).
[7]E. S. Toberer, S. R. Brown, T. Ikeda, S. M. Kauzlarich, and G. J. Snyder, Appl. Phys. Lett. **93**, (2008).
[8]F. Gascoin, S. Ottensmann, D. Stark, S. M. Haile, and G. J. Snyder, Adv. Funct. Mater. **15**, 1860 (2005).
[9]H. Zhang *et al*., J. Chem. Phys. **129**, (2008).
[10]C. Yu *et al*., J. Appl. Phys. **104**, (2008).
[11]E. S. Toberer, A. F. May, B. C. Melot, E. Flage-Larsen, and G. J. Snyder, Dalton Trans. **39**, 1046 (2010).
[12]G. Cordier, E. Czech, M. Jakowski, and H. Schaefer, Rev. Chim. Miner. **18**, 9 (1981).
[13]E. S. Toberer, A. Zevalkink, N. Crisosto, and G. J. Snyder, Adv. Funct. Mater. **20**, 4375 (2010).
[14]S. Park, E. Choi, W. Kang, and S. Kim, J. Mater. Chem. **12**, 1839 (2002).
[15]I. Todorov, D. Y. Chung, L. Ye, A. J. Freeman, and M. G. Kanatzidis, Inorg. Chem. **48**, 4768 (2009).
[16]S.-J. Kim, J. R. Ireland, C. R. Kannewurf, and M. G. Kanatzidis, J. Solid State Chem. **155**, 55 (2000).
[17]S. R. Brown, E. S. Toberer, T. Ikeda, C. A. Cox, F. Gascoin, S. M. Kauzlarich, and G. J. Snyder, Chem. Mater. **20**, 3412 (2008).
[18]A. D. LaLonde, T. Ikeda, and G. J. Snyder, Rev. Sci. Instrum. **82**, (2011).
[19]G. Kresse and J. Hafner, Phys. Rev. B **47**, 558 (1993).
[20]G. Kresse and J. Furthmuller, Comput. Mater. Sci. **6**, 15 (1996).
[21]J. P. Perdew, K. Burke, and M. Ernzerhof, Phys. Rev. Lett. **77**, 3865 (1996).
[22]G. Kresse and D. Joubert, Phys. Rev. B **59**, 1758 (1999).
[23]Y. I. Ravich, B. A. Efimova, and I. A. Smirnov, *Semiconducting Lead Chalcogenides* (Plenum, New York, 1970).
[24]R. D. Shannon and C. T. Prewitt, Acta Crystallogr., Sect. B: Struct. Crystallogr. Cryst. Chem. **25**, 925 (1969).
[25]F. J. DiSalvo, *Science* **295**, 703 (1999).
[26]Y. Pei, X. Shi, A. Lalonde, H. Wang, L. Chen, G. J. Snyder, "Convergence of electronic bands for high performance bulk thermoelectrics," Nature (to be published).
[27]A. F. May, E. S. Toberer, A. Saramat, and G. J. Snyder, Phys. Rev. B **80**, 125205 (2009).
[28]H. J. Goldsmid, *Applications of Thermoelectricity* (J. Wiley and Sons, New York, 1960).
[29]D. G. Cahill and R. O. Pohl, Annu. Rev. Phys. Chem. **39**, 93 (1988).
[30]G. A. Slack, *Solid State Physics* (Academic, New York, 1979), Vol. 34.
[31]M. Roufosse and P. G. Klemens, Phys. Rev. B **7**, 5379 (1973).
[32]E. S. Toberer, A. Zevalkink, and G. J. Snyder, "Phonon engineering through crystal chemistry" Chem. Mater. (to be published).